Chemistry & Biology, Vol. 10, 1103–1113, November, 2003, ©2003 Elsevier Science Ltd. All rights reserved. DOI 10.1016/j.chembiol.2003.10.011

Structure-Based Discovery of Potassium Channel Blockers from Natural Products: Virtual Screening and Electrophysiological Assay Testing

Hong Liu,[1] Yang Li,[1] Mingke Song,[1] Xiaojian Tan, Feng Cheng, Suxin Zheng, Jianhua Shen, Xiaomin Luo, Ruyun Ji, Jianmin Yue,* Guoyuan Hu,* Hualiang Jiang,* and Kaixian Chen
Center for Drug Discovery and Design
State Key Laboratory of Drug Research
Shanghai Institute of Materia Medica
Shanghai Institutes for Biological Sciences
Chinese Academy of Sciences
Shanghai 201203
People's Republic of China

Summary

Potassium ion (K^+) channels are attractive targets for rational drug design. Based upon a three-dimensional model of the eukaryotic K^+ channels, the docking virtual screening approach was employed to search the China Natural Products Database. Compounds were ranked according to the relative binding energy, favorable shape complementarity, and potential of forming hydrogen bonds with the K^+ channel. Four candidate compounds found by virtual screening were investigated by using the whole-cell voltage-clamp recording in rat dissociated hippocampal neurons. When applied extracellularly, compound 1 markedly depressed the delayed rectifier K^+ current (I_K) and fast transient K^+ current (I_A), whereas compounds 2, 3, and 4 exerted a more potent and selective inhibitory effect on I_K. Intracellular application of the four compounds had no effect on both the K^+ currents.

Introduction

K^+ channels play important roles in regulating a variety of cellular processes in both electrically excitable and nonexcitable cells, such as control of action potential and excitability in nerve and muscle cells, regulation of hormone secretion, cell volume, and T lymph cell activation [1–3]. Nine unique families of voltage-gated K^+ channels have been discovered [4]. The best-characterized K^+ channels are derived from homologs of the *Drosophila* K^+ channel genes, *Shaker*, *Shab*, *Shaw*, and *Shal*, which exist in mammalian tissues and were assigned as Kv1, Kv2, Kv3, and Kv4, respectively [4–6]. Each of these channels has multiple subfamily members. Their structures are predicted to be similar, with six transmembrane-spanning domains (S_1–S_6), a pore-forming region located between transmembrane segments S_5 and S_6, and intracellular amino and carboxyl termini [7]. The pore-forming region is conserved among K^+ channels [7]. Among the K^+ channels, the KcsA K^+ channel from the bacterium *Streptomyces lividans* was the first, with its three-dimensional (3D) structure elucidated with X-ray crystallography at 3.2 Å resolution [8]. These experimental data support the hypothetical model described above by localizing the pore region and by orienting the two transmembrane-spanning domains of the bacterial channel [8]. In addition, this structure provides a unifying hypothesis that explains ion selectivity and the fast rates of ion conduction through the pore.

Natural products have long been recognized as an important source of therapeutically effective agents. One hundred fifty-seven of the five hundred twenty new drugs approved between 1983 and 1994 were natural products or derived from natural products, and more than 60% of antibacterials and anticancer drugs originated from natural products [9]. Meanwhile, the completion of the human genome suggests that there are 30,000 to 40,000 genes and at least as many proteins. Many of these proteins are potential targets for drug screening; popular estimates are in the range of 2000 to 5000 [10, 11]. Therefore, natural products will offer unprecedented opportunities for finding novel low molecular weight lead structures that are active against a wide range of assay targets [9]. The challenge is how to access the natural chemical diversity. Collecting all the available natural product compounds and screening them randomly target by target is unpractical, because it will cost a lot of money and is also time consuming in isolating and screening compounds. Virtual screening (VS) has the potential to solve this problem [12–15]. VS, by using docking, shows great promise in lead or active compound discovery [12, 14, 16–18]. It was demonstrated that VS enriched the hit rate by thousands-fold over random screening [16].

Structure-based ligand design has led to the development of compounds that are currently in clinical trials or on the market [19, 20]. In most cases, methods for structure-based lead generation were based on computational descriptions of a binding site, as in the coordinates of atoms or pharmacophores, and also based on techniques to search for the configurational and conformational space of a candidate molecule in the binding site, evaluating potential energy and/or scoring binding affinity [20]. Some natural compounds that interact with the surface pocket of K^+ channels might block K^+ ion efflux [21], and thus could possibly be developed as new pharmaceuticals [22]. In order to identify novel K^+ channel binding molecules, we have developed a computational virtual screening approach to mine the available natural structure data. The advantages of VS for discovery of novel K^+ channel blockers are prominent, as high-throughput screening is immature in this field [23]. Using the VS approach, we found 14 natural compounds of relatively lower binding energy, favorable shape complementarity, and/or potential in forming hydrogen bonds with K^+ channel. We examined four candidate compounds available in our laboratory using whole-cell voltage-clamp recording, and all of them exerted potent inhibitory effects on K^+ channels in rat hippocampal neurons.

*Correspondence: jmyue@mail.shcnc.ac.cn (J.Y.), gygu@mail.shcnc.ac.cn (G.H.), jiang@iris3.simm.ac.cn (H.J.)
[1] These authors contributed equally to this work.

Results and Discussion

Identification of Compounds by Virtual Screening

Against the K^+ channel structural model, we searched the CNPD database [24] with 50,000 compounds by using the program DOCK 4.0 [25, 26]. The extracellular and pore binding site formed by tetramer in the model structure of eukaryotic K^+ channels was used as the target site for virtual screening. In particular, we focused on potential ligands that interact with the residues surrounding the entry of the "ion-selective filter" of K^+ channels [27] so that the selected compounds may plug the filter. In the database search, conformational flexibility of the small molecules was taken into account. The small molecules were ranked according to their scores calculated by using the energy scoring function in the DOCK program. The top 200 candidate molecules with the best scores were considered as possible K^+ channel inhibitors for further study.

However, docking programs and scoring functions have a tendency to generate a significant number of false positives [13]. Accordingly, to reduce the false positives in compound selection, the structures of the complexes of the top 200 molecules selected from DOCK screening with the K^+ channels were optimized in the Sybyl6.7 [28] environment by running a SPL [28] program written by ourselves, and the interaction energies (ΔE_{bind}) were recalculated by using a more sophisticated method, molecular mechanics force field (see Equation 1 in Experimental Procedures). The root-mean-square deviation (rmsd) values between the conformations of the 200 structures selected by DOCK4.0 and that minimized by Sybyl are shown in Supplemental Table S1 (available at http://www.chembiol.com/cgi/content/full/10/11/1103/DC1); the Sybyl structures only depart slightly from the corresponding DOCK structures, and most of the rmsd values are less than 1 Å. This suggests that the Sybyl optimizations made a small adjustment for the DOCK structures. The interaction energies of these 200 molecules with K^+ channels calculated by DOCK range from −28.0 to −15.1 kcal/mol, and those calculated by Sybyl are from −61.4 to −20.1 kcal/mol (Figures 1A and 1B). The DOCK interaction energies are generally in agreement with the Sybyl interaction energies (Figure 1B), indicating the reasonability of the DOCK screening results. Because Sybyl interaction energies were calculated based on the optimized DOCK structures by using molecular mechanics force field, the former may be more robust than the later. Accordingly, the candidate molecules for bioassay were selected according to the Sybyl interaction energies (Figure 1B). Moreover, the shape complementarity and potential in forming hydrogen bonds with K^+ channels were also considered in the molecule selection. Thus, we selected 14 compounds (**1–14**) from the left part of Figure 1B as the candidates for bioassay. Then the binding free energies of these 14 molecules with K^+ channels were estimated using AutoDock3.0 [29, 30]. The rmsd values of the Sybyl minimized structures and AutoDock structures of these 14 molecules are also shown in Supplemental Table S1 (available at *Chemistry & Biology*'s website); they indicate that AutoDock makes a further adjustment for the Sybyl optimized structures. The number of the selected compounds and their binding affinities from different scoring functions are listed in Table 1.

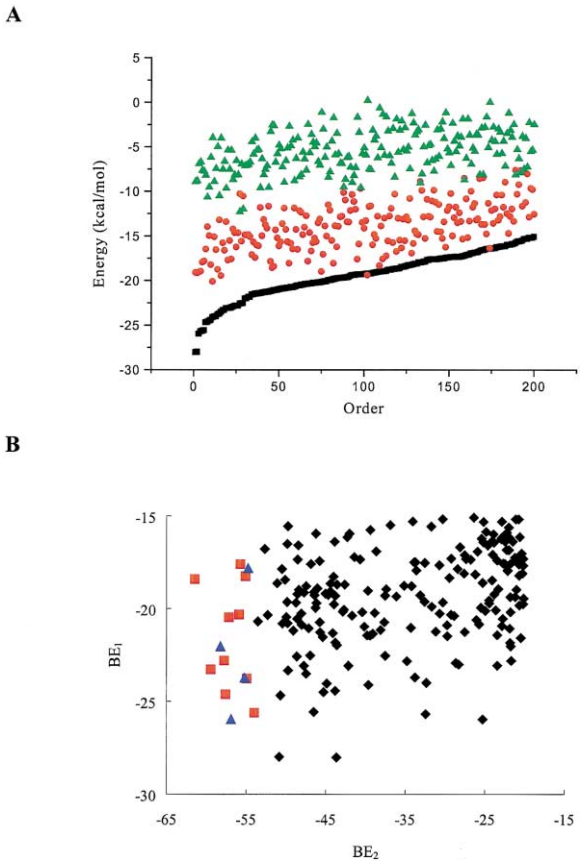

Figure 1. Binding Energies of the Top 200 Compounds

(A) Binding energies of the top 200 compounds ranked from the CNPD database by DOCK 4.0. (black squares, total binding energy; red circles, van de Waals energy; green triangles, electrostatic energy).

(B) DOCK predicted binding energies (BE_1) versus Sybyl calculated binding energies (BE_2) for the top 200 compounds (blue triangles, compounds **1–4**; red squares, compounds **5–14**; black diamonds, compounds **15–200**).

Two hundred six compounds showed potent K^+ channel inhibitory activity in the MDL Drug Data Report (MDDR) database [31]. Ten of them are in clinical trails. We calculated their logP values by using the XLOGP program [32]. The results are shown in Supplemental Figure S1A (available at *Chemistry & Biology*'s website). The logP values of 70% K^+ channel inhibitors in the MDDR database range from 0 to 6. Nine of the clinical compounds show logP values from 2 to 6. The logP values of the 200 DOCK-selected compounds from CNPD are shown in Supplemental Figure S1B. Ninety-six percent of these compounds have logP values from 0 to 6. The logP values of the finally selected 14 compounds range from 0.26 to 6.19 (Table 1). This indicates that our selected compounds have a similar hydrophobic property to the existing K^+ inhibitors collected in MDDR.

On the basis of virtual screening and logP prediction, we intended to select these 14 compounds for bioassay.

Table 1. Binding Energies, Actual Ranks, and XlogP Values of the 14 Compounds Selected from the 200 Candidates

Compound	BE_1[a]	R_1[a]	BE_2[b]	R_2[b]	BE_3[c]	R_3[c]	XlogP
1	−17.82	140	−54.772	13	−9.19	11	0.77
2	−22.04	32	−58.257	3	−8.66	12	3.23
3	−25.97	3	−56.892	7	−7.35	14	1.91
4	−23.73	16	−55.224	10	−7.52	13	0.70
5	−18.41	127	−61.446	1	−15.4	2	3.09
6	−23.28	20	−59.442	2	−14.82	3	2.98
7	−22.81	27	−57.762	4	−12.14	8	0.85
8	−24.63	9	−57.599	5	−13.22	7	2.85
9	−20.47	66	−57.171	6	−14.53	4	1.20
10	−20.32	71	−55.908	8	−13.4	6	0.26
11	−17.60	143	−55.729	9	−10.64	10	0.34
12	−18.25	130	−55.085	11	−11.42	9	3.28
13	−23.78	15	−54.929	12	−16.28	1	4.14
14	−25.62	6	−54.004	14	−13.68	5	6.19

[a] The binding energy (BE_1) and the actual rank (R_1) calculated using DOCK.
[b] The binding energy (BE_2) and the actual rank (R_2) calculated using Sybyl.
[c] The binding energy (BE_3) and the actual rank (R_3) calculated using AutoDock.

Being short of samples for other compounds, only 4 compounds (**1–4**) among the 14 selected molecules were finally obtained for the actual biological testing.

K^+ Channel-Blocking Effects

The actions of compounds **1–4** on K^+ channels were examined by using whole-cell voltage-clamp recording in dissociated hippocampal neurons of rat. In the left panel of Figure 2B, the upper and middle records are the total K^+ current and the delayed rectifier K^+ current (I_K) elicited with two different voltage protocols. The lower record is the subtraction of the middle from the upper one, representing the fast transient K^+ current (I_A). I_K and I_A could be blocked reversibly by tetra-ethyi-ammonium (TEA, $IC_{50} = 3.1 \pm 0.6$ mM) and 4-aminopyridine (4-AP, $IC_{50} = 4.9 \pm 0.6$ mM), respectively [33, 34].

Extracellular application of compounds **1–4** potently inhibited I_K (Figure 2). The IC_{50} values of compounds **1–4** in inhibition of I_K are 125.3 ± 15.3, 3.8 ± 1.4, 90.0 ± 5.9, and 164.8 ± 26.3 μM, respectively, with a rank order of potency of **2**>**3**>**1**∼**4**. However, only compound **1** exerted moderate inhibition on I_A ($IC_{50} = 2.4 \pm 0.3$ mM), whereas compounds **2–4** had no effect on the current at concentrations of nearly 1 mM.

Hippocampal pyramidal neurons are the most extensively studied cell type in the mammalian brain showing the diversity of K^+ channels. At least four voltage-dependent K^+ currents and two Ca^{2+}-activated K^+ currents were characterized in the neurons [35]. In the neurons prepared from 5- to 9-day-old rats, however, only the main voltage-dependent K^+ currents I_K and I_A could be detected [36]. Moreover, the two currents can be easily separated through a signal subtraction procedure based on their distinct kinetic properties [33, 34], avoiding the interference caused by addition of TEA or 4-AP in isolation of the currents. In this study, we demonstrate that the natural compounds **1–4**, found by docking screening, block K^+ channels with different preferences and potencies, indicating that our strategy for targeting structure-based virtual screening is feasible. Furthermore, our results show that compounds **2–4** are potent and selective blockers of I_K. At a concentration of nearly 1 mM, the three compounds abolished I_K but had no detectable effects on I_A (Figures 2D–2F). In contrast, compound **1** inhibited both I_A and I_K (Figures 2B and 2C).

K^+ Channel Binding Site Mapping

Extracellularly applied chemicals, like verapamil, could diffuse through the membrane and block the K^+ channels at an internal binding site [37, 38]. To determine the binding site of the four natural products to the K^+ channel, external or internal site, the effects of intracellular application of compounds **1–4** on the K^+ currents were investigated. Compounds **1–4** were added in the pipette solution with concentrations that could inhibit I_K by more than 75% in extracellular application. The compounds diffused into the recorded neuron immediately after the patch membrane ruptured [39]. However, the amplitude of I_K in the intracellular application group and control group showed no difference during the 12 min after the patch membrane ruptured (Figure 3). Additionally, intracellular application of compounds **1–4** had no effect on I_A (data not shown). The result suggests that compounds **1–4** bind to an extracellular site of the K^+ channels, thus blocking the K^+ currents.

To confirm the above conclusion, membrane-impermeable quaternary *N*-methyl-compounds of **1–4** were prepared and tested both extracellularly and intracellularly by adopting the method of Rauer et al. [37, 38]. When applied extracellularly, the inhibitory action to the K^+ channel of the *N*-methyl-compounds is similar to that of natural products **1–4**. (1) The IC_{50} values of the *N*-methyl-compounds in inhibition of I_K are 244.2 ± 13.8, 8.9 ± 1.4, 45.9 ± 3.0, and 490.2 ± 19.1 μM, respectively, which are close to those of compounds **1–4**. The rank order of the inhibitory potency of the *N*-methyl-compounds is *N*-methyl-**2** > *N*-methyl-**3** > *N*-methyl-**1** > *N*-methyl-**4**, which is exactly the same as the order of the natural products. (2) Similar to the natural products, only *N*-methyl-**1**, applied extracellularly, resulted in moderate inhibition on I_A ($IC_{50} = 1.9 \pm 0.01$ mM), whereas the other three *N*-methyl compounds showed no effect on I_A at concentrations of nearly 1 mM. Intracellular application of the *N*-methyl compounds at concentrations

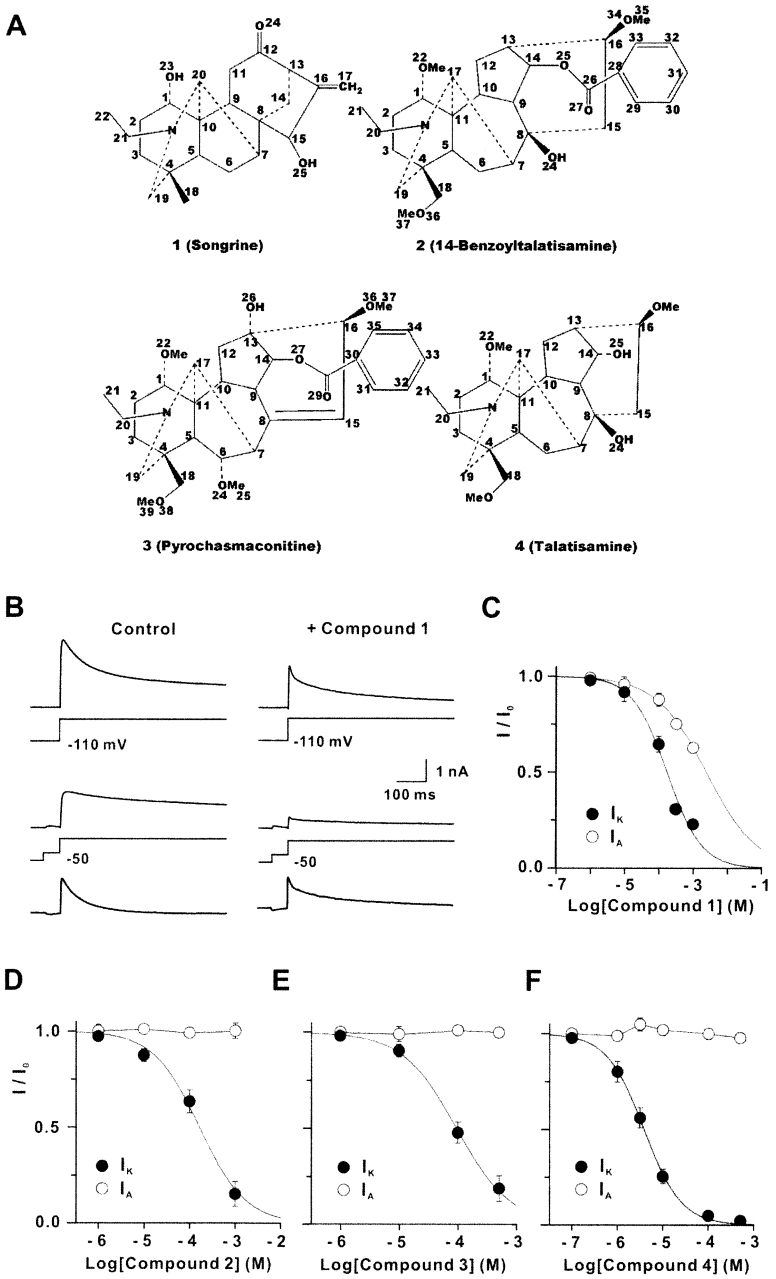

Figure 2. Effects of Extracellularly Applied Compounds **1–4** on Voltage-Dependent K^+ Currents in Rat Hippocampal Neurons

(A) The structures of compounds **1–4**.

(B) The left panel shows the subtraction procedure used to separate the delayed rectifier K^+ current (I_K) and fast transient K^+ current (I_A). The upper record is the total K^+ current evoked by a depolarizing pulse to +60 mV following a prepulse to −110 mV; the middle record is I_K evoked by a similar voltage protocol with a 50 ms step to –50 mV inserted after the prepulse; and the lower record is the subtraction of the middle record from the upper one, representing I_A. Traces at the bottom of upper and middle records are voltage command pulses. The right panel shows that extracellular application of 300 μM compound **1** inhibited both I_K and I_A.

(C) Concentration-response curves of compound **1** in inhibition of I_K and I_A. Each symbol represents the mean ± SEM (n = 5–12).

(D–F) Compounds **2, 3,** and **4** selectively blocked I_K without effect on I_A in rat hippocampal neurons. (D) shows concentration-response curves of compound **2** in inhibition of I_K and I_A (n = 7–12); (E) shows concentration-response curves of compound **3** in inhibition of I_K and I_A (n = 3–8); (F) shows concentration-response curves of compound **4** in inhibition of I_K and I_A (n = 5–8). The peak amplitude of I_A and amplitude of I_K at 300 ms after the start of the depolarizing pulse were measured by constructing the concentration-response curves in (C)–(F).

that could inhibit I_K by more than 75% in extracellular application affected neither I_K (see Supplemental Figure S2 at *Chemistry & Biology*'s website) nor I_A (data not shown). These results gave further support to the conclusion that compounds **1–4** do indeed bind to the extracellular site of K^+ channels.

Interaction Models

Figure 4 shows the general interaction models of compounds **1–4** with K^+ channels. Figure 4 was produced by the LIGPLOT program [40] based on the DOCK simulation and Sybyl optimization results. Hydrogen bond and hydrophobic interactions play important roles in the binding of these four compounds and K^+ channels; the detailed interaction models are presented in Figure 4 and Table 2. Compounds **1–4** form 2, 3, 3, and 2 hydrogen bonds with the K^+ channel, respectively. The hydrogen bonding strength (reflected by the hydrogen bond number) is in agreement with the inhibitory potency that the K^+ channel inhibitory activities (IC_{50} for inhibiting I_K) of compounds **2** and **3** are higher than that of compounds **1** and **4** (Table 2). Compounds **1–4** interact with the K^+ channel, adopting 32, 18, 22, and 26 pairs of hydrophobic contacts (Figure 4 and Table 2). The number of hydrophobic contact pairs is not in agreement with the inhibitory potency, indicating that the difference of inhibitory activities of these four compounds might be distinguished by the hydrogen bonding. Structurally, compounds **1–4** are diterpenoid alkaloids and have similar chemical scaffolds. However, comparing the interac-

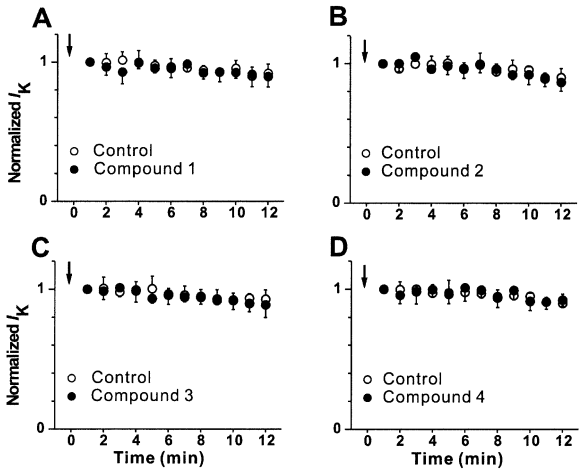

Figure 3. Intracellular Application of Compounds **1–4** on the Delayed Rectifier K^+ Current (I_K) in Rat Hippocampal Neurons

In each panel, the normalized I_K is plotted against the time of intracellular application of the compounds. Each symbol represents the mean ± SEM (n = 5). The arrow indicates the time when patch membrane ruptured. (A), compound **1** (300 μM); (B), compound **2** (50 μM); (C), compound **3** (300 μM); (D), compound **4** (1 mM). The concentrations chosen for intracellular application were above the IC_{75} values (causing 75% inhibition of I_K) of the same compounds in external application.

tion models of these compounds with the K^+ channel, it can be seen that the carbonyl group of the substituted 14-benzoyl moiety of compounds **2** and **3** forms two hydrogen bonds with Ser57(C) and Thr82(C). This might be one of the reasons that the activities of compounds **2** and **3** are higher than that of compounds **1** and **4**.

Significance

There has been no report of the computational screening targeting of K^+ channels. Here, we have demonstrated the protocol that predicts the binding of small molecules to eukaryotic *Shaker* K^+ channels' 3D model. We used an effective compound ranking strategy to select compounds from the natural product database CNPD [24]. The top 200 molecules were obtained by a shape complementarity scoring function in DOCK [25, 26]; the complexes of these 200 candidates with the K^+ channel model were optimized by molecular mechanics encoded in Sybyl [28], and the interaction energies were calculated; and, finally, these compounds were reestimated using AutoDock [29, 30], and the binding free energies were predicted. In addition, the logP values of these 200 molecules were predicted by the XlogP program [32]. Considering the three kinds of energy scoring data and the XlogP values, we selected 14 candidate compounds for bioassay. Although we only obtained four compounds (1–4) for electrophysiological assay due to lack of samples, the results demonstrated the efficiency of our strategy of virtual screening. Each of these four compounds shows inhibitory activity to K^+ channels. Their I_K blocking activities are ~20–1000 times higher than that of TEA. In addition, the predictive binding affinities of these four compounds are not the highest among the 14 candidates; one may find more potent K^+ channel blockers among the remaining 10 compounds. Furthermore, the interaction features of these four compounds binding with K^+ channels were mapped, providing a clear clue for further modification of these natural products. The strategy used in this paper provides a method for quickly discovering new K^+ channel blockers from large databases, especially given that high-throughput screening of K^+ channel is currently unavailable.

Experimental Procedures

Virtual Screening

3D Model of Eukaryotic Shaker *K^+ Channel*

The 3D model of eukaryotic *Shaker* K^+ channel was generated based on the crystal structure of Kcsa K^+ channel [8]. The KcsA channel is a tetramer containing four identical subunits arranged symmetrically around the central pore (P)[8]. Each subunit consists of two transmembrane α helices (TM1 and TM2), linked by a short stretch of ~30 amino acids, that form a helical pore and an extracellular loop (known as the turret). The four TM2 helices are arranged in such a way that they form the poles of an inverted teepee [8]. The crystal structure provides a solid framework for the models of the K^+-selective channels, and for the first time gives indisputable evidence that the ion permeation pathway across the membrane is indeed at the center of four identical subunits that cluster around the narrowest part of the pore formed by the P loop [8]. Mutagenesis studies suggest that the "ion-selective filter" is located at the external end of the pore and is formed by the conserved signature sequence, TXXTXGY(F)G, within the pore region [41]. KcsA shares signature sequences with eukaryotic K^+ channels that are responsible for ion selectivity and pore formation. Based on the observation that TEA can bind to the external part of the K^+ pore in all three of the channel types, voltage-activated, Ca^{2+}-activated, and inward-rectifier K^+ channels, the structure of the outer pore of K^+ channels appears to be conserved, in spite of the lack of conservation of the sequence in the P region [41, 42]. Further evidence is provided by experiments conducted by MacKinnon et al. showing that the KcsA K^+ channel pore structure and the extracellular entryway are very similar to that of eukaryotic voltage-gated K^+ channels, such as the *Shaker* K^+ channel from *Drsophila* and vertebrate voltage-gated K^+ channels [41, 43, 44]. We can therefore generate a 3D model for the eukaryotic *Shaker* K^+ channels according to the X-ray crystal structure of KcsA [8] and the mutagenesis results [41, 43, 44]. We have successfully used this approach in modeling the 3D structures of the eukaryotic K^+ channels for studying the binding of K^+ channels with scorpion toxins Lq2 [45] and P05 [46].

For the 3D structure modeling, the sequences of eukaryotic *Shaker* K^+ and KcsA channels were isolated from the SwissProt database (entries P08510 and Q54397, respectively). The sequence alignment of KcsA and eukaryotic channels with the *Shaker* K^+ channels was carried out using the GCG software [47]. The 3D model of the eukaryotic *Shaker* K^+ channels was constructed based on the crystal structure of KcsA K^+ channel recovered from the Protein Data Bank (http://www.rcsb.org/pdb/) (ID code 1BL8) [48]. The side chains of residues Arg27, Ile60, Arg64, Glu71, and Arg117 missed in the current KcsA crystal structure were added using the Biopolymer module of Sybyl 6.7 [28]. Figure 5 shows the sequence alignment of the pore regions of the two K^+ channels, highlighting the mutation residues. The 3D structural model of eukaryotic *Shaker* K^+ channels was generated from mutations of Pro55Glu (P55E), Ala57Ser (A57S), Ile60Lys (I60K), Thr61Ser (T61S), Arg64Asp (R64D), Leu81Met (L81M), and Tyr82Thr (Y82T) on the X-ray crystal structure of the KcsA K^+ channel [8] employing the Biopolymer module of Sybyl. After the coordinate assignment, the preliminary 3D model of eukaryotic *Shaker* K^+ channel was subjected to structure refinement. The side chains of the 3D model were minimized first by fixing the backbone, then the entire 3D structure was optimized. The structures were minimized using 200 steps of steepest descent, followed by Powell

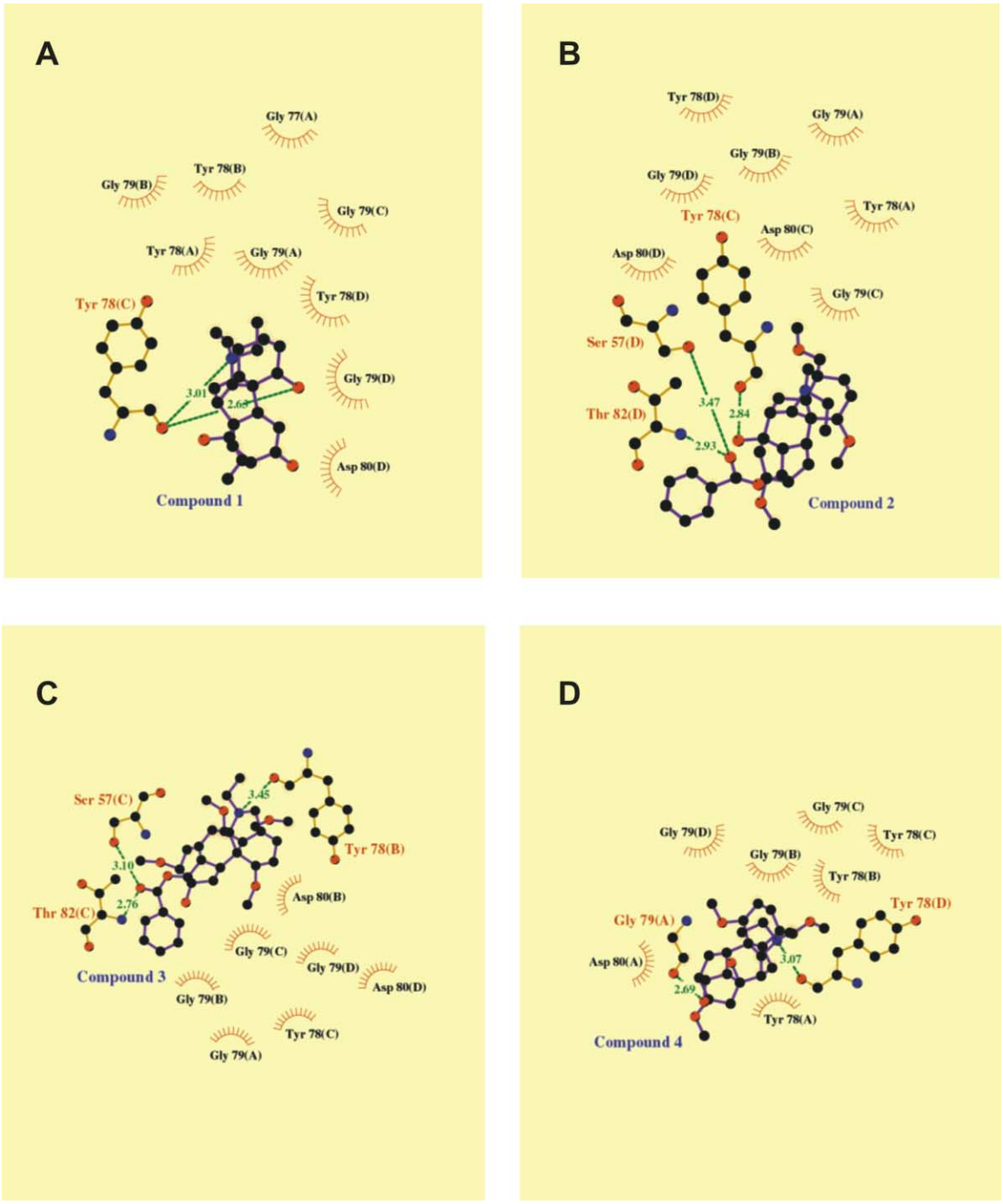

Figure 4. 2D Representatives for the General Interaction Models of Compounds 1-4 with Potassium Ion Channel

This picture was produced by using LIGPLOT program [40]. Dashed lines represent hydrogen bonds, and spiked residues form hydrophobic contacts with the natural products. A, B, C, and D represent the four chains of the K^+ channel.

minimization to a root-mean-square (rms) energy gradient of 0.05 kcal/(mol·Å). Amber force field with Kollman-all-atom charges [49] was employed throughout. Solvation energies were not explicitly considered; however, minimization was performed with a distance-dependent dielectric constant.

The quality of the models was checked by the Prostat program encoded in Insight II [50], which allows protein-specific bond lengths, angles, and dihedral angles to be checked against the corresponding reference values. The cut-off concerning the significant differences for the bond lengths, bond angles, and dihedral angles from the reference value was set up at the default value, 5 units of standard deviation (SD). For the 3D model, only nine bond angles and seven dihedral angles were identified to be larger than 5 SD; no bond length is larger than 5 SD. The structure superposition of the 3D model with the X-ray structure of KcsA K^+ channel is available in Supplemental Figure S3 at http://www.chembiol.com/

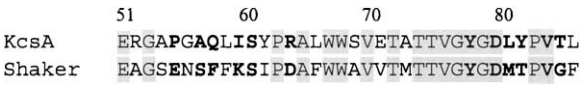

Figure 5. Sequence Alignment of the KcsA and Shaker K^+ Channel Pore Regions

Boldface letters indicate amino acids where mutations influence ligand binding. The conserved residues are shaded. The sequences are KcsA/*S. Lividans* (SwissProt entry Q54397) and Shaker/*Drosophila melanogaster* (SwissProt entry P08510).

cgi/content/full/10/11/1103/DC1. For all the nonhydrogen atoms, the rmsd between the crystal structure of KcsA K^+ channel and the 3D model is 0.374 Å, and the rmsd between the binding pockets of the two K^+ channel structures is 0.415 Å, indicating the reliability of the 3D model. We can therefore use this 3D model in further virtual screening.

Virtual Screening by Molecular Docking

The optimized 3D model of eukaryotic K^+ channel was used as a target for virtual screening on the China Natural Product Database [24], which was developed by Shanghai Institute of Materia Medica, Chinese Academy of Sciences, collaborating with Neotrident Technology Lid. (http://www.neotrident.com). The CNPD database contains structural and biological information of more than 50,000 natural compounds. Some of them are unpublished or were published in Chinese journals that have not been appreciated by academia and companies.

No scoring function has been developed so far that may reliably and consistently predict a ligand-protein binding mode and binding affinity [51, 52]. Therefore, heuristic docking and consensus scoring strategies are often used in virtual screening; i.e., the different docking and scoring methods are applied to evaluate the screening results. In the present study, the program DOCK4.0 [25, 26] was employed for the primary screening. Binding experiments [53–55] indicated that the TEA extracellular binding site is around the conserved signature motif TXXTXGYG of K^+ channels. Residues around the motif TXXTXGYG of the K^+ channel at a radius of 5 Å was isolated for constructing the grids of docking screening, and the pocket composed by these residues is larger enough to include residues of the binding site. During the docking calculation, Kollman-all-atom charges [49] were assigned to the protein, and Geisterger-Hückel charges [56–58] were assigned to the small molecules in the CNPD database due to lack of proper Kollman charges. The conformational flexibility of the natural products from the database was considered in the docking searching.

The DOCK suite of programs is designed to find possible orientations of a ligand in a "receptor" site [25, 26]. The orientation of a ligand is evaluated with a shape scoring function and/or a function approximating the ligand-receptor binding energy. The shape scoring function is an empirical function resembling the van der Waals attractive energy. The ligand-receptor binding energy is taken to be approximately the sum of the van der Waals and electrostatic interaction energies. After the initial orientation and scoring evaluation, a grid-based rigid body minimization is carried out for the ligand to locate the nearest local energy minimum within the receptor binding site. The position and conformation of each docked molecule were optimized using single anchor search and torsion minimization method of DOCK4.0 [25, 26]. Thirty configurations per ligand building a cycle and 50 maximum anchor orientations were used in the anchor-first docking algorithm. All docked configurations were energy minimized using 100 maximum iterations and 1 minimization cycle.

Then, the whole structures of the complexes of the top 200 molecules with the K^+ channel were optimized automatically by running a SPL program written by ourselves encoded into Sybyl [28] environment to adjust the orientation and interaction. The minimization method and parameter setup are the same as that adopted in the minimization for the 3D model construction of the K^+ channel. Tripos force field [28] was employed for the ligands; calculations were performed with a dielectric constant of 5 to simulate the solvation effect of the ligands in the protein environment. The binding energies (ΔE_{bind}) between each molecule and K^+ channel were calculated by using Equation 1,

$$\Delta E_{bind} = E_{complex} - E_{channel} - E_{mol}, \quad (1)$$

where $E_{complex}$, $E_{channel}$, and E_{mol} are, respectively, the total energies of the complexes, the K^+ channel, and the small molecules. Atoms of the small molecules and K^+ channel were assigned with Gasteiger-Hückel [56–58] and Kollman-All charges [49], respectively.

Next, the top 200 molecules were analyzed on the basis of binding energy, shape complementarity, and potential in forming hydrogen bonds with the K^+ channel. Fourteen compounds (**1–14**) were finally selected for bioassay. Before that, the binding free energies and the binding modes of these 14 compounds with the K^+ channel were calculated and modeled by using the advanced docking program AutoDock 3.0 [29, 30]. In the AutoDock calculations, the Lamarckian genetic algorithm (LGA) [30] was applied to search the binding orientation and conformation of each candidate molecule interacting with K^+ channel. In general, the LGA described the relationship between candidate molecules and K^+ channel by the translation, orientation, and conformation of candidate molecules. A Solis and Wets local search [59] performed the energy minimization on a user-specified proportion of the population. The number of generation, energy evaluation, and docking runs were set to 370,000, 1,500,000 and 20, respectively. The Kollman-all-atom [49] and Gasteiger-Hückel [56-58] were used for the K^+ channel and candidate molecules, respectively, in the AutoDock simulations. The docked structures of candidate molecules were generated after a reasonable number of evaluations. Typically, five binding energy terms used in the current version of AutoDock 3.0 [29, 30] were included in the scoring function: the van der Waals interaction, represented as a Lennard-Jones 12-6 dispersion/repulsion term; the hydrogen bonding, represented as a directional 12-10 term; the Coulombic electrostatic potential; desolvation upon binding; and the hydrophobic effect (solvent entropy changes at solute-solvent interfaces). Thus, the scoring function was sufficient to rank the candidate molecules in the different levels of binding affinities: binding free energies (ΔGs) and the corresponding inhibitory constant (K_is). Finally, the interaction models of compounds **1–4** with K^+ channel were produced using the LIGPLOT program [40] based on the AudoDock structures (Figure 4).

LogP prediction

Lipophilicity is a major determinant of several aspects of the disposition and biological action of drugs, and its use in new approaches like database searching additionally proves the impact of this physicochemical property [60]. Consequently, there is continual interest in medicinal chemistry in developing methods of deriving logP from molecular structure [60]. XLOGP 2.0, developed by Lai et al. [32], is an atom-additive method for calculating octanol/water partition coefficient (logP). It gives the logP value for a given compound by adding the contributions from component atoms and correction factors as described in Equation 2,

$$\log P = \sum_i a_i A_i + \sum_j b_j B_j, \quad (2)$$

where A_i is the occurrence of the ith atom type, B_j is the occurrence of the jth correction factor, a_i is the contribution of the ith atom type, and b_j is the contribution of the jth correction factor. The coefficients were derived by multivariate regression of a large number of organic compounds. The logP values of the candidate compounds picked out by DOCK were predicted using this program, and the predicted values were compared with the XlogP values of the K^+ inhibitors collected in MDDR database [31].

Compounds for Bioassay

Based on virtual screening, 14 compounds of K^+ channel inhibitor candidates, which are listed in Table 1, were distinguished. Unfortunately, only four samples of these compounds are available in our laboratory, including one diterpenoid alkaloid , songorine (**1**), and three norditerpenoid alkaloids, 14-benzoyltalatisamine (**2**), pyrochasmaconitine (**3**), and talatisamine (**4**). Therefore, we selected these four compounds as probe molecules for electrophysiological assay to test our virtual screening strategy. Compounds **1–4** were isolated from the root of *Aconitum leucostomum* [61, 62], a perennial

Table 2. The Hydrogen-Bonding Pairs and the Hydrophobic Contacts of Compounds 1–4 with the K^+ Channel Derived from AutoDock Simulations

Compound	Interaction	Distance (Å)	Compound Atom	K^+ Channel Residue[a]	K^+ Channel Atom
1	Hydrogen bond	3.01	N	Tyr78(C)	O
		2.63	O23	Tyr78(C)	O
	Hydrophobic contacts	3.84	C22	Tyr78(D)	C
		3.81	C21	Gly79(C)	CA
		3.08	C21	Tyr78(C)	C
		3.75	C21	Tyr78(C)	CA
		3.69	C13	Asp80(D)	CB
		3.50	C13	Asp80(D)	CA
		3.72	C14	Asp80(D)	CA
		3.74	C14	Gly79(D)	C
		3.80	C14	Tyr78(D)	C
		3.36	C12	Asp80(D)	CA
		3.61	C12	Gly79(D)	C
		3.26	C20	Gly79(D)	CA
		3.52	C20	Tyr78(D)	C
		3.84	C11	Gly79(D)	C
		3.56	C19	Gly79(C)	CA
		3.55	C19	Gly79(B)	CA
		3.46	C19	Tyr78(B)	C
		3.48	C18	Gly79(B)	C
		3.53	C18	Gly79(B)	CA
		3.55	C9	Gly79(D)	C
		3.58	C9	Gly79(D)	CA
		3.85	C10	Gly79(D)	CA
		3.82	C3	Gly79(C)	CA
		3.25	C2	Gly79(C)	C
		3.24	C2	Gly79(C)	CA
		3.71	C7	Gly79(A)	C
		3.69	C6	Gly79(A)	CA
		2.96	C7	Gly79(A)	CA
		3.85	C8	Gly79(A)	CA
		3.38	C22	Tyr78(A)	C
		3.82	C22	Tyr78(A)	CA
		3.78	C22	Gly77(A)	C
2	Hydrogen bond	3.47	O27	Ser57(D)	OG
		2.93	O27	Thr82(D)	N
		2.84	O24	Tyr78(C)	O
	Hydrophobic contacts	3.88	C24	Asp80(C)	CB
		3.61	C34	Asp80(D)	C
		3.59	C38	Ser57(D)	CB
		3.82	C33	Ser57(D)	CB
		3.33	C29	Tyr78(D)	C
		3.89	C29	Tyr78(D)	CA
		3.59	C13	Asp80(C)	CA
		3.89	C13	Gly79(C)	C
		3.63	C14	Gly79(B)	CA
		3.33	C11	Gly79(D)	CA
		3.71	C11	Gly79(C)	CA
		3.59	C11	Tyr78(C)	C
		3.31	C10	Gly79(C)	C
		3.26	C10	Gly79(C)	CA
		3.81	C10	Tyr78(C)	CA
		3.18	C12	Gly79(A)	CA
		3.70	C29	Tyr78(A)	C
		3.40	C12	Tyr78(A)	C
3	Hydrogen bond	3.45	N	Tyr78(B)	O
		3.10	O29	Ser57(C)	OG
		2.76	O29	Thr82(C)	N
	Hydrophobic contacts	3.77	C31	Ser57(C)	CB
		3.69	C30	Ser57(C)	CB
		3.84	C21	Tyr78(C)	C
		3.29	C21	Tyr78(B)	C
		3.89	C21	Tyr78(B)	CA

(*continued*)

Table 2. Continued

Compound	Interaction	Distance (Å)	Compound Atom	K^+ Channel Residue[a]	K^+ Channel Atom
		3.85	C20	Gly79(C)	CA
		3.63	C20	Tyr78(C)	C
		3.49	C25	Gly79(B)	C
		3.59	C39	Asp80(D)	CA
		3.21	C39	Gly79(D)	C
		3.61	C39	Gly79(D)	CA
		3.76	C15	Asp80(B)	CB
		3.56	C15	Asp80(B)	CA
		3.78	C17	Gly79(C)	CA
		3.37	C6	Gly79(B)	C
		3.44	C6	Gly79(B)	CA
		3.63	C7	Gly79(B)	C
		3.51	C7	Gly79(B)	CA
		3.76	C7	Tyr78(B)	C
		3.60	C9	Gly79(C)	C
		3.81	C9	Gly79(C)	CA
		3.54	C19	Gly79(C)	CA
4	Hydrogen bond	3.07	N	Tyr78(D)	O
		2.69	O25	Gly79(A)	O
	Hydrophobic contacts	3.62	C21	Tyr78(B)	C
		3.87	C20	Gly79(D)	CA
		2.99	C20	Tyr78(D)	C
		3.67	C20	Tyr78(D)	CA
		3.19	C18	Gly79(C)	C
		3.01	C18	Gly79(C)	CA
		3.79	C6	Gly79(B)	C
		3.46	C6	Gly79(B)	CA
		3.67	C7	Gly79(B)	C
		3.05	C7	Gly79(B)	CA
		3.67	C19	Gly79(D)	CA
		3.69	C19	Gly79(C)	CA
		3.63	C19	Tyr78(C)	C
		3.36	C2	Gly79(D)	C
		3.32	C2	Gly79(D)	CA
		3.32	C14	Asp80(A)	CA
		3.89	C9	Asp80(A)	CA
		3.57	C14	Gly79(A)	C
		3.31	C9	Gly79(A)	C
		3.82	C10	Gly79(A)	C
		3.36	C20	Gly79(A)	CA
		3.23	C17	Gly79(A)	CA
		3.66	C9	Gly79(A)	CA
		3.62	C21	Tyr78(A)	C
		3.43	C20	Tyr78(A)	C
		3.66	C17	Tyr78(A)	C

[a] A, B, C, and D represent the four chains of the K^+ channel.

herb distributed in the Gansu and Xinjiang provinces of China. The purity of these compounds is over 98%, and isolation and spectral data of these four compounds has been described elsewhere [61, 62].

Electrophysiological Assay

Preparation of Dissociated Hippocampal Neurons

Dissociated CA1 hippocampal neurons were prepared from 5- to 9-day-old Sprague-Dawley rats as described previously [63]. Briefly, minislices (500 μm) of the hippocampal CA1 region were cut in oxygenated ice-cold dissociation solution containing 82 mM Na_2SO_4, 30 mM K_2SO_4, 5 mM $MgCl_2$, 10 mM HEPES, and 10 mM glucose (pH 7.3). The slices were incubated in dissociation solution containing 3 mg/ml protease XXIII at 32°C for 8 min. The solution was then replaced with dissociation solution containing 1 mg/ml trypsin inhibitor type II-S and 1 mg/ml bovine serum albumin. The slices were allowed to cool to room temperature under an oxygen atmosphere. Before recording, the slices were triturated using a series of fire-polished Pasteur pipettes with decreasing tip diameters. Dissociated neurons were placed in a recording dish and perfused with external solution containing 135 mM NaCl, 5 mM KCl, 1 mM $CaCl_2$, 2 mM $MgCl_2$, 10 mM HEPES, 10 mM glucose, and 1 μM tetrodotoxin (pH 7.3).

Whole-Cell Recording

Whole-cell voltage-clamp recording was made from large pyramidal-shaped neurons using an Axopatch 200A amplifier (Axon Instruments, USA) at 21–23°C. The electrodes (tip resistance 3–5 MΩ) were filled with pipette solution containing 125 mM potassium gluconate, 20 mM KCl, 2 mM $MgCl_2$, 1 mM $CaCl_2$, 10 mM HEPES, and 10 mM EGTA (pH 7.3). The holding potential was −50 mV. Voltage protocols were provided by pClamp 6.2 software via a DigiData-1200A interface (Axon Instruments). The total K^+ currents (I_T) were elicited by depolarizing command pulses to +60 mV in 10 mV steps following a hyperpolarizing prepulse of 400 ms to −110 mV. The delayed rectifier K^+ currents (I_K) were elicited by a similar protocol in which a 50 ms interval at −50 mV was inserted after the prepulse.

Subtraction of I_K from I_T revealed the fast transient K^+ current (I_A) [34, 35, 63]. Current records were filtered at 2–10 KHz and sampled at frequencies of 10–40 KHz. Series resistance was compensated by 75%–85%. Linear leak and residual capacitance currents were subtracted on-line using a P/6 protocol. For extracellular application, the compounds were dissolved in external solution. The solution was directly applied to the recorded neuron using RSC-100 Rapid Solution Changer with an 18-tube head (BioLogic Co., France). For intracellular application, the compounds were isosmotically substituted for glucose in pipette solution and diffused into the recorded neuron immediately after patch membrane ruptured [39].

The IC_{50} values of the compounds were calculated by using the software Microcal Origin 6.0 [64]. Data are presented as mean ± SEM.

Supplemental Data

The LogP values of the K^+ channel inhibitors in the MDDR database and the top 200 compounds picked from the CNPD database are shown in Figure S1. Effects of intracellular application of *N*-methyl-compounds **1–4** on the delayed rectifier K^+ current (I_K) in rat hippocampal neurons are shown in Figure S2. The structure superposition of the 3D model of eukaryotic *Shaker* K^+ channel with the X-ray crystal structure of KcsA K^+ channel is shown in Figure S3. The RMSDs between the Sybyl minimized structures and DOCK structures of the top 200 candidate molecules and the rmsds between the Sybyl minimized structures and AutoDock structures of the 14 candidate molecules are shown in Table S1. The structures and plant sources of the other ten candidates identified by virtual screening from the CNPD databases that have not been tested by the electrophysiological method are listed in Table S2. All Supplemental Data is available at http://www.chembiol.com/cgi/content/full/10/11/1103/DC1.

Acknowledgments

The authors thank Professor I.D. Kuntz and Professor Arthur J. Olson for their kindness in offering us the DOCK 4.0 and AutoDock 3.0.3 programs. We gratefully acknowledge financial support from National Natural Science Foundation of China (Grants 20102007, 29725203, and 20072042), the State Key Program of Basic Research of China (Grants 2002CB512802 and 2002CB512807), and the 863 Hi-Tech Program of China (Grants 2002AA233061, 2001AA235051, and 2001AA235041).

Received: October 25, 2002
Revised: September 1, 2003
Accepted: September 8, 2003
Published: November 21, 2003

References

1. Kaczorowski, G.J., and Garcia, M. (1999). Pharmacology of voltage-gated and calcium-activated potassium channels. Curr. Opin. Chem. Biol. *3*, 448–458.
2. Garcia, M.L., Hanner, M., Knaus, H.G., Koch, R., Schmalhofer, W., Slaughter, R.S., and Kaczorowski, G.J. (1997). Pharmacology of potassium channels. Adv. Pharmacol. *39*, 425–471.
3. Clare, J.J., Tate, S.N., Nobbs, M., and Romanos, M.A. (2000). Voltage-gated sodium channels as therapeutic targets. Drug Discov. Today *5*, 506–520.
4. Biggin, P.C., Roosild, T., and Choe, S. (2000). Potassium channel structure: domain by domain. Curr. Opin. Struct. Biol. *10*, 456–461.
5. Zhou, Y.F., Morais-Cabral, J.H., Kaufman, A., and MacKinnon, R. (2001). Chemistry of ion coordination and hydration revealed by a K^+ channel-Fab complex at 2.0 Å resolution. Nature *414*, 43–48.
6. Robertson, B. (1997). The real life of voltage-gated K^+ channels: more than model behavior. Trends Pharmacol. Sci. *18*, 474–483.
7. Lu, Z., Klem, A.M., and Ramu, Y. (2001). Ion conduction pore is conserved among potassium channels. Nature *413*, 809–813.
8. Doyle, D.A., Cabral, J.M., Pfuetzner, R.A., Kuo, A., Gulbis, J.M., Cohen, S.L., Chait, B.T., and MacKinnon, R. (1998). The structure of the potassium channel: molecular basis of K^+ conduction and selectivity. Science *280*, 69–77.
9. Harvey, A. (2000). Strategies for discovering drugs from previously unexplored natural products. Drug Discov. Today *5*, 294–300.
10. Hopkins, A.L., and Groom, C.R. (2002). The druggable genome. Nat. Rev. Drug Discov. *1*, 727–730.
11. Dean, P.M., Zanders, E.D., and Bailey, D.S. (2001). Industrial-scale, genomics-based drug design and discovery. Trends Biotechnol. *19*, 228–292.
12. Shoichet, B.K., McGovern, S.L., Wei, B., and Irwin, J.J. (2002). Lead discovery using molecular docking. Curr. Opin. Chem. Biol. *6*, 439–446.
13. Schneider, G., and Böhm, H.J. (2002). Virtual screening and fast automated docking methods. Drug Discov. Today *7*, 64–70.
14. Waszkowycz, B., Perkins, T.D.J., Sykes, R.A., and Li, J. (2001). Large-scale virtual screening for discovering leads in the post-genomic era. IBM Systems J. *40*, 360–376.
15. Richards, W.G. (2002). Virtual screening using grid computing: the screensaver project. Nat. Rev. Drug Discov. *1*, 551–555.
16. Doman, T.N., McGovern, S.L., Witherbee, B.J., Kasten, T.P., Kurumbail, R., Stallings, W.C., Connolly, D.T., and Shoichet, B.K. (2002). Molecular docking and high-throughput screening for novel inhibitors of protein tyrosine phosphatase-1B. J. Med. Chem. *45*, 2213–2221.
17. Lind, K.E., Du, Z., Fujinaga, K., Peterlin, B.M., and James, T.L. (2002). Structure-based computational database screening, in vitro assay, and NMR assessment of compounds that target TAR RNA. Chem. Biol. *9*, 185–193.
18. Grüneberg, S., Stubbs, M.T., and Klebe, G. (2002). Successful virtual screening for novel inhibitors of human carbonic anhydrase: strategy and experimental confirmation. J. Med. Chem. *45*, 3588–3602.
19. Kuntz, I.D., Meng, E.C., and Shoichet, B.K. (1994). Structure-based molecular design. Acc. Chem. Res. *27*, 117–123.
20. Wang, J.L., Liu, D.X., Zhang, Z.J., Shan, S., Han, X.B., Srinivasula, S.M., Croce, C.M., Alnemri, E.S., and Huang, Z.W. (2000). Structure-based discovery of an organic compound that binds Bcl-2 protein and induces apoptosis of tumor cells. Proc. Natl. Acad. Sci. USA *97*, 7124–7129.
21. Naranjo, D., and Miller, C. (1996). A strongly interacting pair of residues on the contact surface charybdotoxin and a Shaker K^+ channel. Neuron *16*, 123–130.
22. Carmeliet, E.M.K. (1998). Antiarrhythmic drugs and cardiac ion channels: mechanisms of action. Prog. Biophys. Mol. Biol. *70*, 1–72.
23. Perozo, E., MacKinnon, R., Bezanilla, F., and Stefani, E. (1993). Gating currents from a nonconducting mutant reveal open-closed conformations in Shaker K^+ channels. Neuron *11*, 353–358.
24. Shanghai Institute of Materia Medica, Chinese Academy of Sciences and Neotrident Systems Pte Ltd. (2000). China Natural Products Database (http://www.neotrident.com).
25. Ewing, T., and Kuntz, I.D. (1997). Critical evaluation of search algorithms for automated molecular docking and database screening. J. Comput. Chem. *18*, 1175–1189.
26. Kuntz, I.D. (1992). Structure-based strategies for drug design and discovery. Science *257*, 1078–1082.
27. MacKinnon, R., Cohen, L., Kuo, A., Lee, A., and Chait, B.T. (1998). Structural conservation in prokaryotic and eukaryotic potassium channels. Science *280*, 106–109.
28. Tripos Associates, St. Louis, MO. (2000). Sybyl, Version 6.7.
29. Morris, G.M., Goodsell, D.S., Huey, R., and Olson, A.J. (1996). Distributed automated docking of flexible ligands to protein: parallel application of AutoDock 2.4. J. Comput. Aided Mol. Des. *10*, 293–304.
30. Morris, G.M., Goodsell, D.S., Halliday, R.S., Huey, R., Hart, W.E., Belew, R.K., and Olson, A.J. (1998). Automated docking using Lamarckian genetic algorithm and empirical binding free energy function. J. Comput. Chem. *19*, 1639–1662.
31. MDL Information Systems, Inc. (2001). MDL Drug Data Report (MDDR) database (http://www.prous.com/product/electron/mddr.html).
32. Wang, R.X., and Lai, L.H. (1997). Calculating partition coeffi-

cients of peptides by the addition method. J. Chem. Inf. Comput. Sci. *37*, 615–621.
33. Klee, R., Ficker, E., and Heinemann, U. (1995). Comparison of voltage-dependent potassium currents in rat pyramidal neurons acutely isolated from hippocampal regions CA1 and CA3. J. Neurophysiol. *74*, 1982–1995.
34. Numann, R.E., Wadman, W.J., and Wong, R.K.S. (1987). Outward currents of single hippocampal cells obtained from the adult guinea-pig. J. Physiol. *393*, 331–353.
35. Storm, J.F. (1993). Functional diversity of K currents in hippocampal pyramidal neurons. Semin. Neurosci. *5*, 79–92.
36. Santos, A.I., Wadman, W.J., and Costa, P.F. (1998). Sustained potassium currents in maturing CA1 hippocampal neurons. Brain Res. Dev. Brain Res. *108*, 13–21.
37. Rauer, H., and Grissmer, S. (1996). Evidence for an internal phenylalkylamine action on the voltage-gated potassium channel KV1.3. Mol. Pharmacol. *50*, 1625–1634.
38. Rauer, H., and Grissmer, S. (1999). The effect of deep pore mutations on the action of phenylalkylamines on the Kv1.3 potassium channel. Br. J. Pharmacol. *127*, 1065–1074.
39. Hu, G.Y., Biro, Z., Hill, R.H., and Grillner, S. (2002). Intracellular QX-314 causes depression of membrane potential oscillations in lamprey spinal neurons during fictive locomotion. J. Neurophysiol. *87*, 2676–2883.
40. Wallace, A.C., Laskowski, R.A., and Thornton, J.M. (1995). LIGPLOT: A program to generate schematic diagrams of protein-ligand interactions. Protein Eng. *8*, 127–134.
41. Heginbotham, L., Abramson, T., and MacKinnon, R.A. (1992). A functional connection between the pores of distantly related ion channels as revealed by mutant K^+ channels. Science *258*, 1152–1155.
42. Lucchesi, K., Ravindran, A., Young, H., and Moczydlowski, E. (1989). Analysis of the blocking activity of charybdotoxin homologs and iodinated derivatives against Ca^{2+}-activated K^+ channels. J. Membr. Biol. *109*, 269–281.
43. Escobar, L., Root, M.J., and MacKinnon, R. (1993). Influence of protein surface charge on the bimolecular kinetics of a potassium channel peptide inhibitor. Biochemistry *32*, 6982–6987.
44. Lu, Z., and MacKinnon, R. (1997). Purification, characterization, and synthesis of an inward-rectifier K^+ channel inhibitor from scorpion venom. Biochemistry *36*, 6936–6940.
45. Cui, M., Shen, J.H., Briggs, J.M., Luo, X.M., Tan, X.J., Jiang, H.L., Chen, K.X., and Ji, R.Y. (2001). Brownian dynamics simulations of interaction between scorpion toxin Lq2 and potassium ion channel. Biophys. J. *80*, 1659–1669.
46. Cui, M., Shen, J.H., Briggs, J.M., Fu, W., Wu, J., Zhang, Y., Luo, X., Chi, Z., Ji, R., Jiang, H., et al. (2002). Brownian dynamics simulations of the recognition of the scorpion toxin P05 with the small conductance calcium-activated potassium channels. J. Mol. Biol. *318*, 417–428.
47. GCG. (2000). Wisconsin Package Version *10*, 0.
48. Bernstein, F.C., Koetzle, T.F., Williams, G.J., Meyer, E.E., Jr., Brice, M.D., Rodgers, J.R., Kennard, O., Shimanouchi, T., and Tasumi, M. (1977). The protein data bank: a computer-based archival file for macromolecular structures. J. Mol. Biol. *112*, 535–542.
49. Weiner, S.J., Kollman, P.A., Nguyen, D.T., and Case, D.A. (1986). An all-atom force field for simulations of proteins and nucleic acids. J. Comput. Chem. *7*, 230–252.
50. Accelrys Molecular Simulations Inc., San Diego, CA. (2000). InsightII, Version 2000.
51. Muegge, I., and Rarey, M. (2001). Small molecule docking and scoring. In Reviews in Computational Chemistry, K.B. Lipkowitz and D.B. Boyd, eds. (New York: John Wiley & Sons), pp. 1–60.
52. Charifson, P.S., Corkery, J.J., Murcko, M.A., and Walters, W.P. (1999). Consensus scoring: a method for obtaining improved hit rates from docking databases of three-dimensional structures into proteins. J. Med. Chem. *42*, 5100–5109.
53. Kavanaugh, M.P., Varnum, M.D., Osborne, P.B., Christie, M.J., Busch, A.E., Adelman, J.P., and North, R.A. (1991). Interaction between tertaethylammonium and amino acid residues in the pore of cloned voltage dependent potassium channels. J. Biol. Chem. *266*, 7583–7587.
54. Kavanaugh, M.P., Hurst, R.S., Yakel, J., Varnum, M.D., Adelman, J.P., and North, R.A. (1992). Multiple subunits of a voltage-dependent potassium channel contribute to the binding site for tetraethylammonium. Neuron *8*, 493–497.
55. MacKinnon, R., and Yellen, G. (1990). Mutations affecting TEA blockade and ion permeation in voltage-activated K^+ channels. Science *250*, 276–279.
56. Gasteiger, J., and Marsili, M. (1980). Iterative partial equalization of orbital electronegativity-A rapid access to atomic charges. Tetrahedron *36*, 3219–3228.
57. Marsili, M., and Gasteriger, J. (1980). π charge distribution from molecular topology and π orbital electronegativity. Croat. Chem. Acta *53*, 601–614.
58. Purcell, W.P., and Singer, J.A. (1967). Brief review and table of semiempirical parameters used in the Hückel molecular orbital method. J. Chem. Eng. Data *12*, 235–246.
59. Solis, F.J., and Wets, R.J.B. (1981). Minimization by random search techniques. Math. Oper. Res. *6*, 19–30.
60. Mannhold, R., and Waterbeemd, H. (2001). Substructure and whole molecule approaches for calculating log P. J. Comput. Aided Mol. Des. *15*, 337–354.
61. Yue, J.M., Xu, J., Zhao, Q.S., and Sun, H.D. (1996). Diterpenoid alkaloids from *Aconitum Leucostomum*. J. Nat. Prod. *59*, 277–279.
62. Yue, J.M., Jun, X., and Chen, Y.Z. (1994). C19-Diterpenoid alkaloids of *Aconitum Kongboense*. Phytochemistry *35*, 829–831.
63. Li, Y., and Hu, G.Y. (2002). Huperzine A, a nootropic agent, inhibits fast transient potassium current in rat dissociated hippocampal neurons. Neurosci. Lett. *324*, 25–28.
64. Microcal Software, Inc. (1999). Origin Version 6.0 (http://www.originlab.com/).